Biointerface Research in Applied Chemistry
Open-Access Journal (ISSN: 2069-5837)

Article
Volume 13, Issue 3, 2023, 201
https://doi.org/10.33263/BRIAC133.201

Fabrication and Characterization of Polycaprolactone with Retinoic Acid and Cerium Oxide for Anticancer Applications

Magda Alahmmar [1], Praseetha Prabhakaran [2,*], Saravana Jaganathan [3,4,5], Nik Ahmad Nizam Nik Malek [6]

1 School of Biosciences, Faculty of Science, Universiti Teknologi Malaysia, 81310 Johor Bahru, Johor, Malaysia
2 Department of Biosciences, Faculty of Science, Universiti Teknologi Malaysia, 81310 Johor Bahru, Johor, Malaysia
3 Department of Engineering, Faculty of Science and Engineering, University of Hull, Hull HU6 7RX, UK
4 Centre for Artificial Intelligence and Robotics, Universiti Teknologi Malaysia, Kuala Lumpur 54100, Malaysia
5 School of Electrical Engineering, Faculty of Engineering, Universiti Teknologi Malaysia, Johor Bahru 81310, Malaysia
6 Centre for Sustainable Nanomaterials (CSNano), Ibnu Sina Institute for Scientific and Industrial Research (ISI-ISIR), Universiti Teknologi Malaysia (UTM), 81310 UTM Johor, Malaysia; niknizam@utm.my (N.A.N.N.M.);
* Correspondence praseetha@utm.my (P.P.);

Scopus Author ID 55171540800
Received: 20.04.2022; Accepted: 16.05.2022; Published: 31.05.2022

Abstract: In the present study, poly (ε-caprolactone) (PCL) composite electrospun nanofibers were fabricated by combining PCL, retinoic acid (RA), and cerium oxide (CeO_2). The parameters processing of material fibers by electrospinning were optimized to obtain PCL-based electrospun nanofiber to be used in drug delivery. The results showed that combined solvents and polymer concentration were found to play key roles in determining the morphology of nanofiber. A single solvent (Dimethylformamide DMF, 100%) favored the beads' formation, whereas beadless fibers were produced with mixed solvents(DMF, chloroform, and methanol). The formation of beads was clearly inhibited due to an increased concentration from 10 to 15% w/v of the polymer. Nanofibers of PCL, PCL/RA, PCL/CeO_2, and PCL/RA/CeO_2 were fabricated and characterized using the combined techniques of SEM (scanning electron microscopy), FTIR (Fourier transform infrared), XRD (X-ray diffraction), TGA (thermogravimetric analysis), contact angle measurements and AFM (atomic force microscopy). The SEM micrographs of RA/CeO_2 loaded PCL nanofibers exhibited similar morphology, and none of them showed bead formation or the presence of RA or CeO_2 on the surface of the nanofiber matrices. The nanofibers loaded with 0.5% RA/CeO_2 drug have the highest diameter (130 ± 33 nm), and the pure PCL nanofibers showed the smallest diameter (74 ± 20 nm) among all the drug-loaded samples evaluated. Also, the XRD analysis displayed the very low crystallinity of RA/CeO_2 in PCL loaded with RA/CeO_2. The result shows that the drug-loaded nanofiber has similar thermal stability to the PCL nanofiber, indicating that the addition of RA and CeO_2 decreases the hydrophobicity. The drug-loaded nanofiber has higher surface roughness than the PCL nanofiber, according to AFM data. Based on the results, PCL/RA/CeO_2 nanofiber is considered a potential material for drug delivery applications.

Keywords: electrospinning; polycaprolactone; retinoic acid; cerium oxide.

1. Introduction

Electrospinning is an emergent technology that is inexpensive, versatile, and simple and can produce fibers with ultrafine particles having diameters ranging from a few nanometres (nm) to a few micrometers (μm) and with controllable morphology at the surface [1, 2]. The

Coulomb force produces these fibers and electrostatic repulsion owing to the applied external electric field onto a polymer solution. A polymer jet is generated by applying a critical potential between a needle (metallic) and a grounded collector, and the produced nanofibers are collected at the connected device [3-5].

Electrospun nanofibers have applications in several areas like energy-related uses [6], scaffolds for tissue production [7-9], drug delivery [10-13], wound bandages [14-16], vascular implants [17-19], and biosensor products [20]. Nanofibers from electrospinning for carriers in pharmaceuticals recently received increasing interest in the biomedical discipline. Many advantages exist in electrospun nanofibers as delivery vehicles, such as targeted release, high-capacity dosage, efficient encapsulation, large surface area, and the modification options for controlled drug delivery [21, 22]. The polymer nanofiber mats' larger surface area facilitates improved close contact with tissues and therapeutic agents [23]. In addition, biodegradable and biocompatible polymer nanofibers with a size of less than 1 μm are particularly useful in the field of medicine, as these nanomaterials mimic components of the molecular and cellular environment in vivo [24].

Among the many synthetic polymers used in electrospinning, polycaprolactone (PCL) is a biodegradable, semi-crystalline, environmentally friendly, biocompatible polymer with various products of other polymers and good processability. Due to this, U.S. Food and Drug Administration permits its biomedical applications [25-28]. In addition to the above properties, the electrospinning procedure for PCL is easy with the ability to generate drug delivery for a long time [29].

Retinoic acid (RA) is an active vitamin A source, a fat-soluble vitamin that plays a key role in cell growth and differentiation [30]. RA contains retinoids having several natural and synthetic compound derivatives that impact growth, apoptosis, and cell differentiation. Retinoids can induce differentiation and apoptosis in cancer cells through cytotoxic and antioxidant actions, indicating potential anti-cancer chemotherapeutic agents [31]. RA is particularly efficient in treating hematologic and epithelial malignancies, including neck, head, and breast cancers, acute promyelocytic leukemia, and ovarian adenocarcinoma [32]. However, the low stability and poor water solubility of ATRA limit its efficacy. Therefore, delivery in tumor tissue and enhancement of its local concentration within tumors are important problems to be addressed [33].

Cerium oxide (CeO_2) is a rare earth oxide with beneficial properties for humans, especially its antioxidant capacity. It accelerates wound healing by sequestering excess superoxide radicals in cells, thus reducing chronic inflammation [34, 35]. By reducing excess species of reactive oxygen (RO) within cells, the alteration of cellular functionalities is avoided, reducing degenerative diseases such as cancer, diabetes, neurological disorders, cardiovascular diseases, and chronic inflammatory conditions such as rheumatoid arthritis. Recent research suggests that cerium oxide nanoparticles are targeted to treat cancer [36, 37]. A study by Giri *et al*. (2013) showed that cerium oxide nanoparticles (CNPs) produced by wet chemical synthesis could play an essential role in treating ovarian cancer by inhibiting several growth factors like vascular endothelial growth factor. The experiment also showed that CNPs could be combined with other chemotherapeutic agents to improve efficacy and reduce side effects [38].

Studies developed using an innovative system of polycaprolactone (PCL) nanofibers comprising of all-trans retinoic acid (ATRA) and hydroxylated multi-walled carbon nanotubes (MWCNTs- OH) and obtained by electrospinning were reported. It has been reported that the

efficient cytotoxicity on cancer stem cells (CSCs) by combining heat and differentiation therapies. The membranes of nanofiber, when applied to the site after surgical tumor removal, can prevent the recurrence of the tumor [39]. Another study reported the application of air entrapped in nanofibers to improve the drug stability for electrospun fibers of PCL treated with hydrophobic poly (glycerol monostearate-co-ε caprolactone, PGC-C18) polymer and with two other types of anti-cancer drugs. The mutual effect of entrapped air and the superhydrophobic nature of fabricated fibers resulted in less hydrolysis of the drug and more sustained release. RA-loaded lipid core nanocapsules have demonstrated a significant increase in antitumor activities compared to drugs alone. Nanosuspensions improve the photostability of the drug, and chitosan nanoparticles of solid lipids improve the topical delivery of RA [40, 41]. Indeed, many drugs have been incorporated with electrospun materials for tumor treatment and have shown excellent therapeutic potential, for instance, doxorubicin and temozolomide [42, 43]. Thus, in this study, we have shown the effect of electrospinning process parameters (polymer concentration and solvents) on fiber diameters for nanofiber optimization to better design drug delivery scaffolds. RA, and CeO_2 were successfully fabricated with PCL by electrospinning procedure. The morphology and physicochemical structure of the prepared materials were examined by SEM, FTIR, contact angle, TGA, AFM, and XRD. The study aimed to produce and characterize PCL-based electrospun nanofiber incorporated with RA and CeO_2.

2. Materials and Methods

Polycaprolactone with molecular weight (PCL, MW = 80,000 g/mol) was obtained from Sigma, USA. Cerium oxide (CeO_2, QReC) was purchased locally. RA (Retinoic Acid) was supplied from Sigma, USA. Chloroform and methanol were obtained from Merck, Burlington, New Jersey, US, and were all employed with no purification. The apparatus for electrospinning (Progene Link Sdn Bhd, Selangor, Malaysia) was used to produce the fibrous. A grounded static collector drum was used.

2.1. Solution preparation and electrospinning parameters.

2.1.1. Optimization of the composite processing.

The PCL solution prepared was run for electrospun fibers, changing electrospinning process conditions tabulated in Table 1. Several parameters, including PCL concentration, DMF, chloroform, and methanol solvent mixture, were modified to determine the blend composition suitable for the electrospinning.

Table 1. Solvent systems and electrospinning condition.

Solvent system	Concentration (%) (w/v)	Feed rate (ml/hr)	Voltage (+kV)	Needle size (G)	Working Distance (cm)
DMF 100%	PCL 10 %	0.5	12.5	21	15
DMF 100%	PCL 12 %	0.5	12.0	21	15
DMF/Chloroform 1.5: 3.5	PCL 12 %	0.5	13.5	21	15
DMF/Chloroform 1.5: 3.5	PCL 12 % / RA 0.25 %	0.5	15.0	21	15
DMF/Chloroform 1.5: 3.5	PCL 15%	0.5	12.5	21	15
DMF/Chloroform 1.5:3.5	PCL 15 % / CeO2 0.25 %	0.5	13.0	21	15
DMF/Chloroform 1.5 :3.5	PCL 15 % /CeO_2/ RA 0.5 %	0.5	15.0	21	15
Chloroform/ Methanol, 4:1	PCL 15 %	0.5	15.0	21	15

2.1.2. Preparation of PCL and composite solutions.

A homogeneous solution of PCL polymer was prepared to make 15 wt. %, where 0.0750 g of PCL was dissolved in chloroform/methanol (4:1 ratio) under magnetic stirring for 24 h at ambient temperature. Different ratios of RA (0.025, 0.25, and 0.5%) were prepared by dissolving the RA in 3 mL methanol and stirring for 10 min. Similarly, different ratios of CeO_2 (0.025, 0.25, and 0.5%) were prepared by dissolving in 3 mL methanol and stirred for about 24 h at room temperature. To obtain PCL/RA solutions at a ratio of 13:2 (v/v), the prepared solutions (0.025 and 0.25%) were added to the PCL homogenous solutions (15 wt. %) and stirred for a maximum of 1 h. Further, the prepared solutions (0.025 and 0.25%) of CeO_2 were added to the PCL homogenous solutions (15 wt. %) and stirred for about 1 h at room temperature and obtained PCL/CeO_2 solutions at a ratio of 13:2 (v/v). Finally, the solution of PCL/RA/ CeO_2 with a ratio of 13:1:1 v/v% was formed by the addition of the prepared RA solution (0.5 wt. %) and CeO_2 solution (0.5 wt. %) to the PCL solution (homogenous, 15 wt. %) and stirred for about 1 h.

2.1.3. Electrospinning of PCL and composite solutions.

All composite solutions have been electrospun under optimized parameters and constantly prepared. A 15 cm distance between needle tip to collector and 0.5 mL/h flow rate was maintained. An applied voltage employed was kept at 12-15 kV. The electrospinning was conducted at room temperature; then, the fibers were obtained in an aluminum foil perpendicular collector. The collected electrospun PCL-based mats were treated for 48 h under vacuum to remove any probable residual solvents, followed by the fiber's storage in a desiccator prior to characterization.

2.2. Nanofiber characterization.

2.2.1. Scanning Electron Microscopy (SEM).

For the analysis of the morphology of the electrospun nanofibers, SEM analyzer (Hitachi SU8020, Tokyo, Japan) was used. A piece (usually small) of electrospun nanofibers is being gold-coated at various magnifications to attain photomicrographs. SEM images at different magnifications were obtained, and ImageJ software was employed to measure the fiber diameter, size, and distribution, thereby measuring 30 different positions randomly.

2.2.2. Analysis with FTIR spectroscopy.

FTIR spectra of the prepared electrospun fibers were recorded using a Nicolet 5 spectrophotometer (Thermo Fischer Scientific, Waltham, MA, USA) to determine the functional groups in the sample electrospun fibers. The spectra of each sample were measured at a wavenumber range of 4000 to 400 cm^{-1} at ambient temperature using a 4 cm^{-1} setting resolution.

2.2.3. Analysis by X-ray Diffraction (XRD).

XRD analysis was performed to analyze the crystal structural variations of the nanofiber membranes. The X-ray intensity was measured using an XRD machine (Rigaku, Tokyo, Japan) in the 2θ range from 10 to 30° using the radiation of CuKα 1.54 Å at a scan rate of 0.05 s^{-1}.

2.2.4. Thermogravimetric Analysis (TGA).

A TGA Unit (Perkin Elmer, Waltham, MA, USA) was employed to conduct thermal analysis to degrade the nanofibrous membranes. The experiments were conducted under a dry nitrogen atmosphere by applying heat to a small part of the sample with the weight of 3 mg in a temperature range from 30 to1000 °C at an ascending rate of 10 °C min^{-1}.

2.2.5. Contact angle measurements.

Contact angle measurements evaluated the wettability of the fibers with equipment for video contact angle (AST Products, Inc., Billerica, MA, USA) using the sessile water drop method. A droplet (0.5 µL) of water was applied to the electrospun fibers, and their static image and surfaces were recorded using camera video. Computer integrated software was used to measure the manual contact from the snapshotted image, and it was repeated for three trials.

2.2.6. Atomic Force Microscopy (AFM).

AFM unit analyzer (JPK Instruments, NanoWizard®, Berlin, Germany) was employed to investigate the roughness of the surface for the electrospun membranes. The AFM analyses were performed at normal temperature in size of 20 by 20 µm area, and images were collected and documented within the medium mode of 256 by 256 pixels. Using JPKSPM software, the nanofiber was analyzed at different positions in the AFM image.

3. Results and Discussion

3.1. Effect of solvents and polymer concentration on fiber morphology.

Morphology of nanofibers is an important factor for obtaining good bioactivity of the material. Thus appropriate material composition gives the required morphology [44]. As shown in Figure 1, combined solvents and polymer concentration have been found to play crucial roles in determining the image shape of nanofiber. The formation of beads was favored in a single solvent (DMF 100%), whereas fibers with beads were less pronounced for a mixture solvent. The improvement in polymer concentration from 10−15% w/v clearly shows beads formation (Figure 1a-e). These results substantiate the findings of previous research works on electrospinning expressing the relationship between polymer concentration, which is strongly correlated to fiber morphology and solution viscosity [44].

Morphology of any nanofibers largely relies on the properties of the solution, mutual interaction of polymer, and drugs. Conductivity difference, viscosity difference, solvents volatility, and surface tension are important physical properties that affect nanofibers' uniformity [45]. The RA/CeO_2 in DMF/Chloroform mixed solvent had high conductivity and very low viscosity, resulting in high pulling force inside a viscous PCL solution. Also, DMF has very low volatility. As a result, the core solution tends to coagulate, which significantly influences the formation of beads within the nanofiber network. PCL/RA/CeO_2 in Chloroform/Methanol could not demonstrate any significant bead formation because the solvents were more volatile and less conductive to electricity. A similar report was observed by Pillay *et al*. [45].

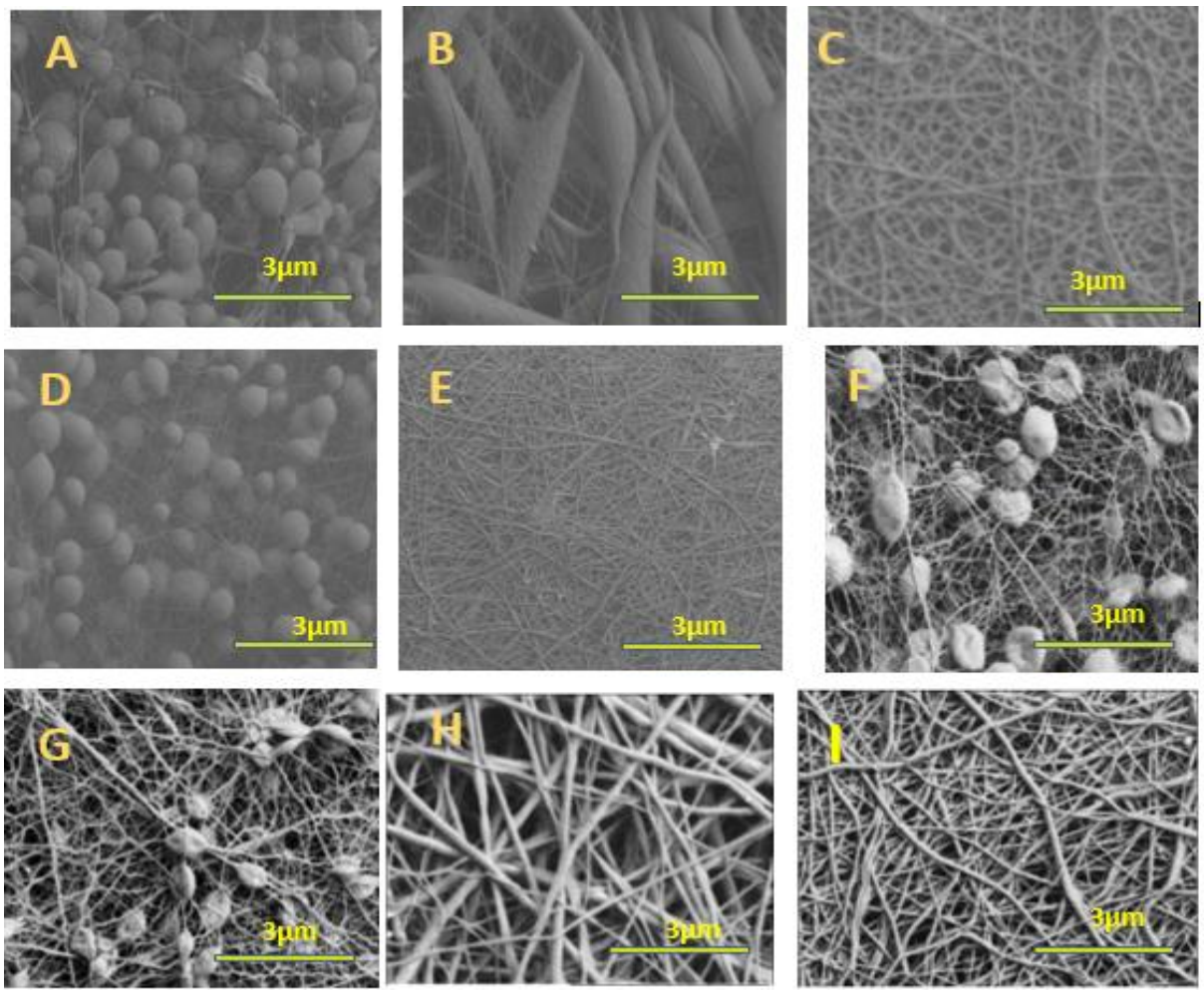

Figure 1. SEM micrographs of different polymer concentrations: (**A**) PCL 10 %; (**B**) PCL 12 % at single solvent (DMF 100%); (**C**) PCL 12 %; (**D**) PCL 12%/RA 0.25%; (**E**) PCL 15%; (**F**) PCL 15 %/CeO_2 0.25 %; (**G**) PCL 15 %/CeO_2/RA 0.5 % at solvent mixture DMF/Chloroform 1.5:3.5; and (**H**) PCL 15 %; (**I**) PCL 15 %/CeO_2/RA 0.5 % at Chloroform/ Methanol 4:1.

3.*2. Characterization of nanofibers.*

3.2.1. SEM Morphology of electrospun nanofibers.

Morphology analysis was done to observe the changes in structure. This work monitored the electrospinning conditions to obtain homogeneous and defect-free fibers. Figure 2(a-f) presents a typical SEM micrograph of PCL, PCL/RA, PCL/CeO_2, and PCL/RA/CeO_2 nanofibers. PCL nanostructured fiber with 74 ± 20 nm average diameter prepared with the optimized electrospinning conditions is presented. Also, when 0.025 wt.% of RA/PCL was added, it turned out that the morphology of the fibers was not modified (Figure 2b), but an increase in particles' diameter can be observed, and the diameter ranges of the nanofiber mats were 105 ± 24 nm. With the RA/PCL (0.25 wt.%) concentration increase, the fiber diameter increases to 116 ± 40 nm. Figure 2(d, e) shows the SEM micrographs of electrospun PCL/CeO_2 nanofibers for the various concentrations of CeO_2 of 0.025 and 0.5 wt.%, respectively. Figures 2(d) and 2(e) show electrospun fibers exhibiting a smooth surface and uniformity in diameters down their lengths, without any noticeable differences when the CeO_2 concentration changes. Thus, the length (in diameters) of fibers composite from the SEM images was estimated using statistical software, as presented in Table 2. It can be seen that the average diameter of the fibers composite reduces with the increase of CeO_2 concentration. This phenomenon could be

a result of the CeO_2 content being raised from 0 to 5 wt.%, the solution's concentration goes higher and the charge density on the surface of the jet increases, generating more charges on the jet's surface, thus raising the tensile force and reducing the fiber diameter [34, 46].

Table 2. Average diameters of PCL, PCL/RA, PCL/CeO_2, and PCL/RA/CeO_2 nanofibers.

Samples	PCL (wt%)	RA (wt%)	CeO_2 (wt%)	Diameter (nm)
S1 (a)	15	-	-	74 ± 20
S2 (b)	15	0.025	-	105 ± 24
S3 (c)	15	0.25	-	116 ± 40
S4 (d)	15	-	0.025	122 ± 24
S5 (e)	15	-	0.25	110 ± 43
S6 (f)	15	0.5	0.5	130 ± 33

When PCL, RA, and CeO_2 were added at appropriate concentrations, the spun fibers appeared smoothly without beads (Figure 2f), while their diameter (average) slowly increased with an RA concentration of 130 ± 33 nm. Thus, all these nanofibers share similar morphology, and none of them showed any formation of bead or any presence of RA or CeO_2 drug on the surface of nanofiber matrices. The 0.5% RA/CeO_2 drug-loaded nanofibers have the highest diameter (130 ± 33 nm), and the pure PCL nanofibers showed the least diameter (74 nm) among all drug-loaded samples. Overall, the SEM images of these nanofibers demonstrated that the nanofiber diameters were slightly increased from the PCL nanofibers to the PCL/RA/CeO_2 nanofibers. Similar observations were also stated by Chen *et al.* (2020) [39].

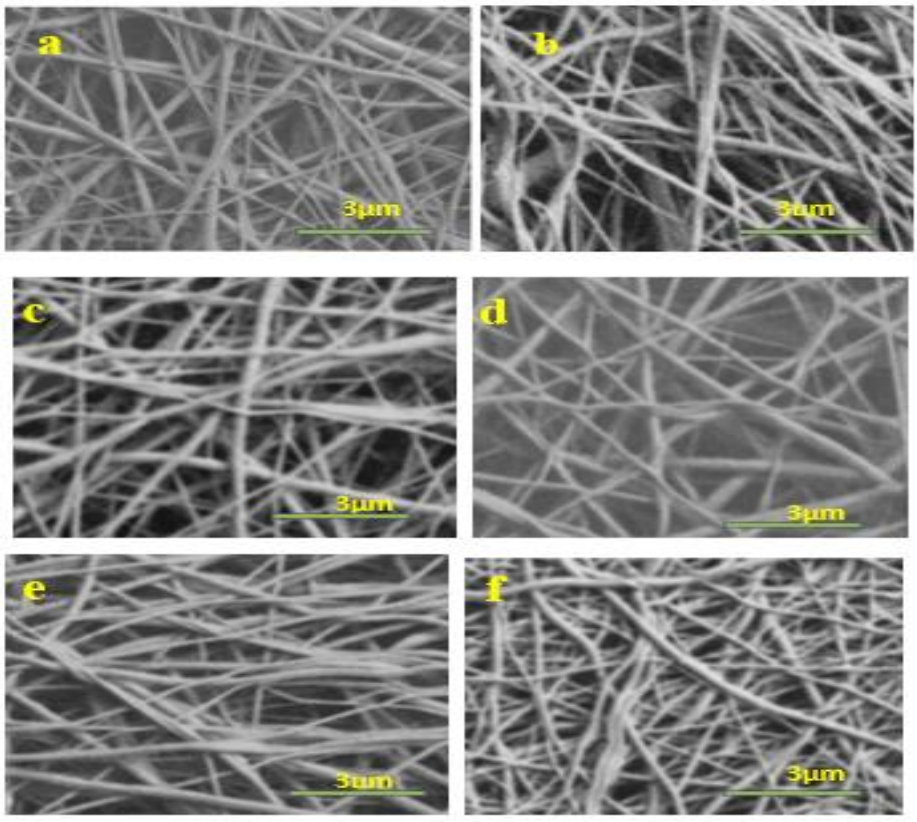

Figure 2. SEM micrographs of electrospun polycaprolactone (PCL) nanofibers prepared with (**a**) PCL no additive; (**b**) 0.025 wt.% RA; (**c**) 0.25wt% RA; (**d**) 0.025 wt.% CeO_2; (**e**) 0.25% CeO_2 wt.%; (**f**) 0.5 wt.% RA & CeO_2.

3.2.2. FTIR spectroscopy analysis.

The results of the infrared analysis of the prepared electrospun scaffolds are presented in Figure 3. The peaks located between 2884 and 2956 cm^{-1} annotated to the pure PCL

corresponds to stretching of the C–H group. The composition of PCL was also clarified with the appearance of C=O stretching vibration at 1740 cm^{-1} and the appearance of C–O stretch with respect to the alcohol group at 962 and 1200 cm^{-1}. In each PCL/RA, PCL/CeO_2, and PCL/RA/CeO_2, no new peak was observed as the compositions of RA and CeO_2 were very low in the nanofibers, leading to over imposed of the PCL functional groups. The existence of the infrared absorption of PCL groups in the spectra of polymeric matrix inclusive of the drug, in addition to the absence of a new band for the PCL/RA, PCL/CeO_2, and PCL/RA/CeO_2, indicated that the structural molecules of the fiber were conserved through the process, essential to yielding the present polymeric drug delivery systems. A similar suggestion was reported by Pereira and her team [47].

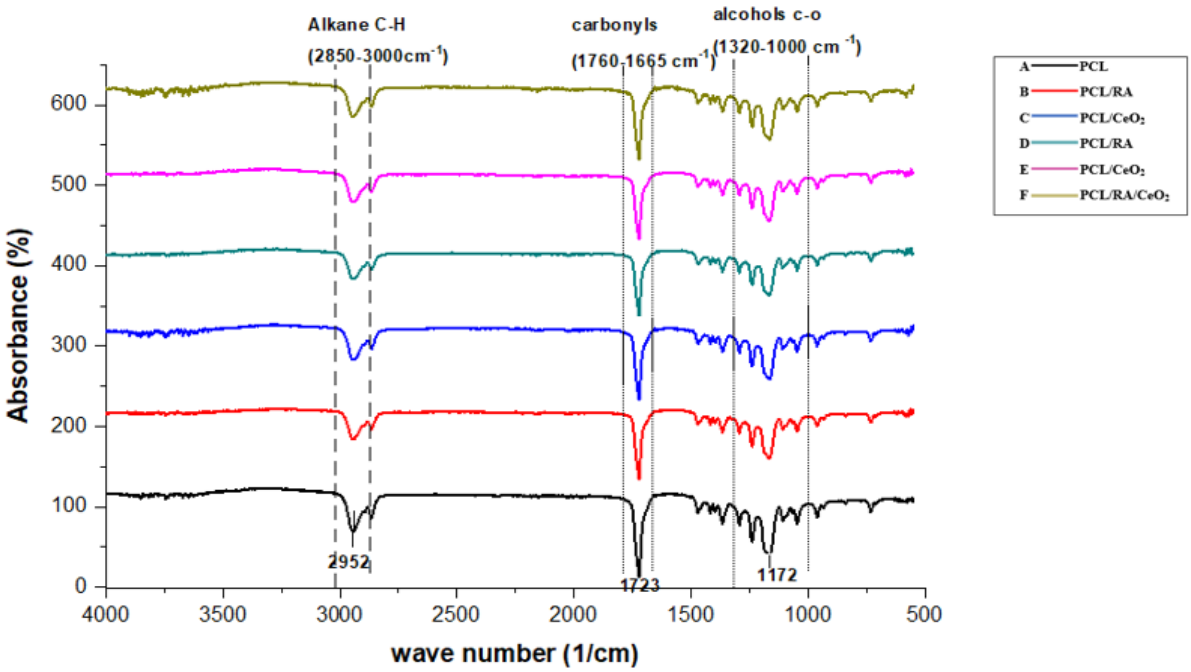

Figure 3. FTIR analysis of (**A**) PCL; (**B**) PCL/RA 0.025 wt.%; (**C**) PCL/CeO_2 0.025 wt.%; (**D**) PCL/RA 0.25 wt.%; (**E**) PCL/CeO_2 0.25 wt.%; (**F**) PCL/RA/CeO_2.

3.2.3. X-Ray Diffraction (XRD).

XRD examination was processed on the electrospun fibers to evaluate their changes in crystalline behavior. Figure 4 shows the XRD patterns of pure PCL, PCL/RA, PCL/CeO_2, PCL/RA, PCL/CeO_2-2, and PCL/RA/CeO_2 labeled as A−F, respectively. In the case of PCL nanofibers, two major peaks appeared at 2θ = 21.3° and 23.8°, ascribed to the diffraction of (110) and (200) lattice planes semi-crystalline. However, PCL/RA (B) 0.025% and PCL/CeO_2 (C) 0.025% showed a similar peak characteristic to the PCL at 23.8°, with reduced intensity. However, compared with PCL/RA (D) 0.25 %, PCL/CeO_2 (E) 0.25%, and PCL/RA/CeO_2 (F) nanofibers, the representative peaks for PCL appeared to have weak intensity. This suggests that RA decreased the PCL crystallites in the fiber by a wider appearance in the region defined as amorphous. For comparison, the amorphous structure (unlike crystalline) is useful for production, tissue growth, and cell adhesion and is extremely fit for biomedical applications [48].

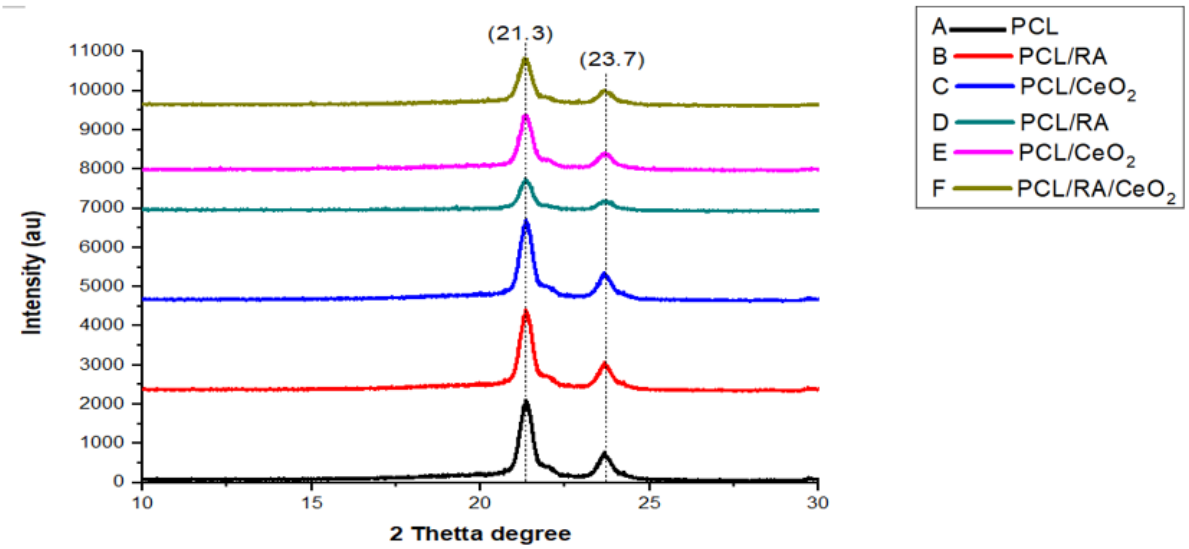

Figure 4. XRD images of (**A**) PCL; (**B**) PCL/RA; (**C**) PCL/CeO_2; (**D**) PCL/RA; (**E**) PCL/CeO_2-2; (**F**) PCL/RA/CeO_2.

3.2.4. Thermogravimetric Analysis (TGA).

Figures 5 and 6 present the TGA and the DTG graphs of the electrospun material displaying the effect of the addition of drug on the PCL's thermal stability and the highest rates of its thermal decomposition with the temperature rise. The characteristic temperatures are presented in Table 3, together with the first and last decomposition temperature, the maximum rate of degradation temperature, including the residue at 550°C; observation has shown that the nanomaterial's first decomposition temperature was decreased to PCL without modification. The pristine PCL showed a starting degradation temperature of 347.5°C and 0.025 wt.% of PCL/RA and 0.025 wt.% of PCL/CeO_2; it was found to be 339.3 and 338.9 °C, respectively. Meanwhile, the increase in the drug content also increased the temperature to be 342.4, 347.2, and 375.8 °C for 0.25 wt.% PCL/CeO_2, 0.25 wt.% PCL/RA, and PCL/RA/ CeO_2, respectively. Thus, the thermal decomposition of the pure PCL was decreased with the integration of 0.025 wt.% of RA and CeO_2, while no significant change in the thermal stability of PCL was induced by the presence of 0.25% of RA, CeO_2, and RA/CeO_2. Additionally, the DTG graphs are shown in Figure 6, which defines the fabricated electrospun membranes' weight loss. The figure suggests that the addition of the RA, CeO_2 and RA/CeO_2 resulted in a slight decrease in this temperature from 394.8 °C of PCL to 392.6, 390.7, 393.3, 391.3, and 394.5 °C for PCL, PCL/RA 0.025 wt.%, PCL/CeO_2 0.025 wt.%, PCL/RA 0.25wt%, PCL/CeO_2 0.25wt%, and PCL/RA/CeO_2, respectively. Therefore, there was no significant change between pure PCL and the incorporation of drugs. Furthermore, the increase of drug content also causes a higher residue of the scaffolds by the end of the degradation than the pristine PCL, which indicates its existence in the composite scaffolds [49].

Table 3. Records of various stages temperature and residue during degradation.

Electrospun scaffold	T_{init} (°C)	T_{fin} (°C)	T_{max} (°C)	Residue at 550 C (mg)
PCL 15%	347.5	413.2	394.8	0.783
PCL/RA 0.025%	339.3	405.8	392.6	1.744
PCL/CeO_2 0.025%	338.9	403.9	390.7	3.104
PCL/RA 0.25%	347.2	411.4	393.3	4.268
PCL/CeO_2 0.25%	342.4	407.2	391.3	3.779
PCL/RA/CeO_2	345.8	411.8	394.5	3.781

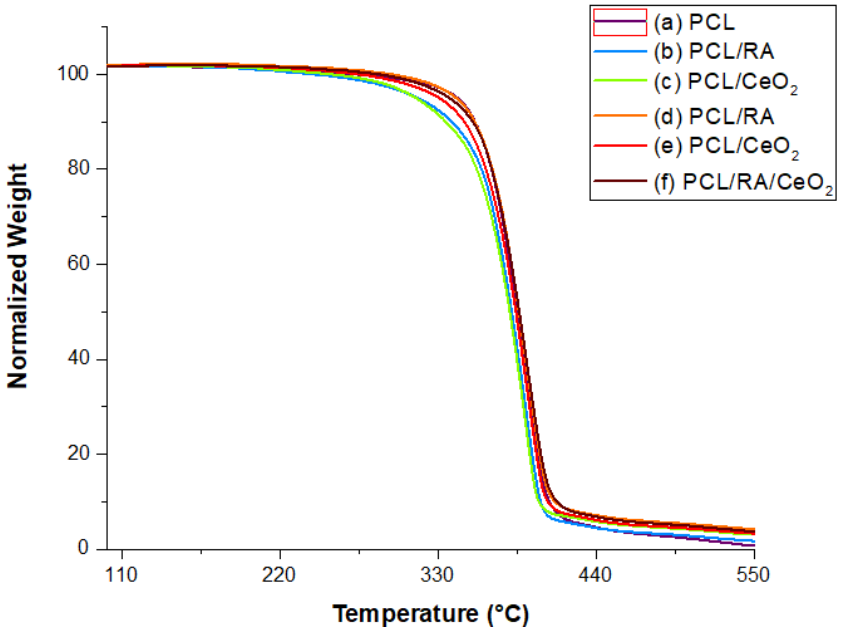

Figure 5. TGA graphs of (**a**) PCL; (**b**) PCL/RA 0.025%; (**c**) PCL/CeO_2 0.025 %; (**d**) PCL/RA 0.25 %; (**e**) PCL/CeO_2 0.25 %; (**f**) PCL/RA/CeO_2.

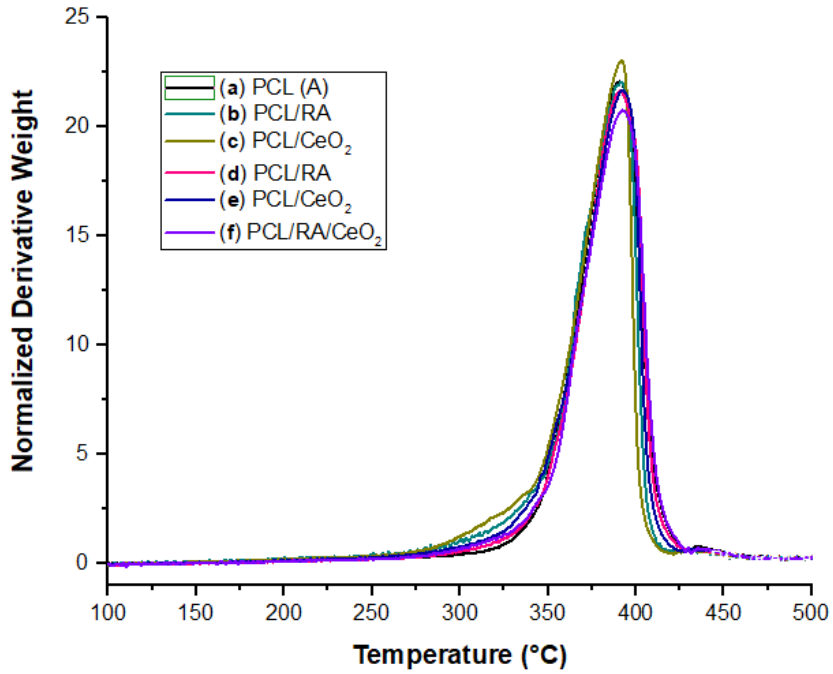

Figure 6. Weight residues of (**a**) PCL; (**b**) PCL/RA 0.025 %; (**c**) PCL/CeO_2 0.025 %; (**d**) PCL/RA 0.25 %; (**e**) PCL/CeO_2 0.25%; (**f**) PCL/RA/CeO_2.

3.2.5. Measurements of contact angle.

The contact angle measurement was conducted to study the changes in the material's mechanical properties (wettability), resulting in the addition of RA and CeO_2. The contact angle profiles of electrospun membranes are shown in Figure 7. The contact angle of the pure PCL nanofibers was 107 ± 2º. While for the PCL/RA 0.025 %, PCL/ CeO_2 0.025 %, PCL/RA 0.25 %, PCL/CeO_2 0.25 %, and PCL/RA/CeO_2, the contact angles were observed to be 101 ± 1º, 107 ± 1º, 97 ± 1º, 105 ± 1º and 80 ± 1º, respectively. In comparison to the pristine PCL membranes, the contact angle of the PCL/RA membranes is reduced in significance when the RA concentration is increased.

Meanwhile, the differences noticed concerning the contact angles of the pure PCL and PCL/CeO_2 are insignificant, indicating that the water membranes' contact angle did not show significant changes. However, it was demonstrated that moderate wettability is more efficient in proteins containing binding cell adhesive, resulting in better cell attachment [50]. It has been reported by Rychter *et al*. (2019) that the decrease of nanofibers' hydrophobicity leads to a higher rate amount of drug release [51].

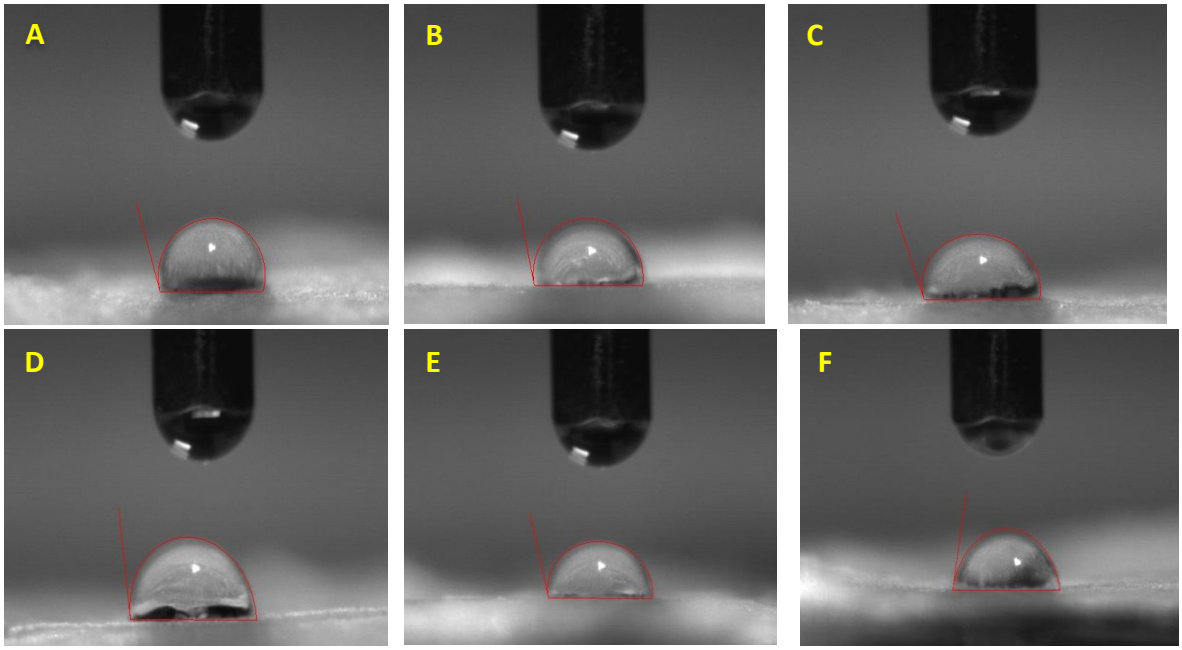

Figure 7 . Contact angle images of (**A**) PCL; (**B**) PCL/RA 0.025%; (**C**) PCL/CeO_2 0.025%; (**D**) PCL/RA 0.25%; (**E**) PCL/CeO_2 0.25%; (**F**) PCL/RA/CeO_2.

3.2.6. Atomic Force Microscopy (AFM).

The AFM procedure was done to analyze the prepared electrospun membranes' surface (roughness) properties, and the images are shown in Figure 8. The PCL surfaces showed an average roughness of 745 nm, and the PCL added with RA 0.025 %, CeO_2 0.025 %, RA 0.25 %, CeO_2 0.25 %, and RA/CeO_2, exhibited a roughness of 780, 764, 813, 792, and 832 nm, respectively. Thus, RA, CeO_2, and RA/CeO_2 have influenced the enhancement of the composite nanofibers' surface roughness. The nanofiber diameter again impacts the surface roughness, where a higher surface roughness was observed with a bigger fiber diameter [52].

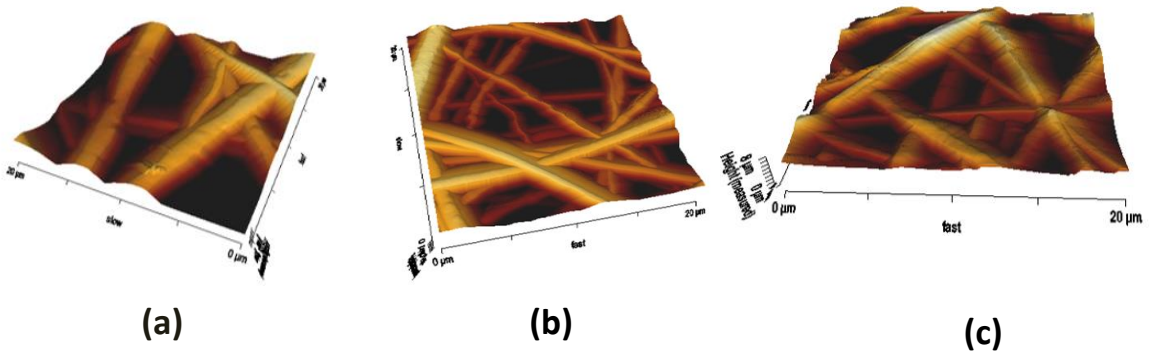

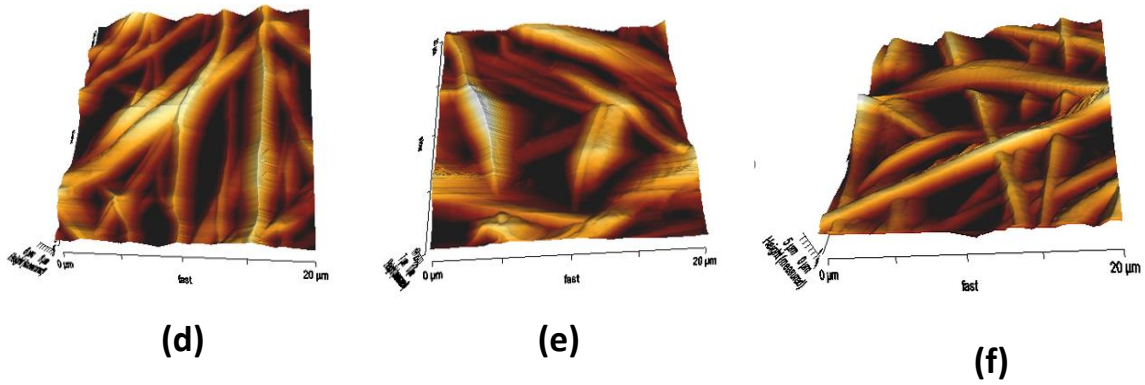

Figure 8. AFM images of (**a**) PCL; (**b**) PCL/RA 0.025 %; (**c**) PCL/CeO_2 0.025 %; (**d**) PCL/RA 0.25 %; (**e**) PCL/CeO_2 0.25 %; (**f**) PCL/RA/CeO_2.

4. Conclusions

PCL nanofibers loaded with RA and CeO_2 were successfully optimized and produced by the electrospinning process using various compositions. Polymer viscosity determined by the concentration, surface tension, and volatility of solvents played a key role in fiber formation. According to the SEM analysis, the smooth and bead-free nanofibers were successfully fabricated, and the solution's concentration has genuinely impacted the fiber diameter. The presence of PCL, RA, and CeO_2 in nanofibers membrane was confirmed by FTIR. Very low crystallinity of RA/CeO_2 was detected in the RA/CeO_2 loaded PCL according to XRD data. The result reveals that the drugs-loaded nanofiber has no significant changes in thermal stability compared to PCL nanofiber and indicates that the addition of RA and CeO_2 decreases the hydrophobicity. Furthermore, the drugs-loaded nanofiber has higher surface roughness than the PCL nanofibers. Based on this research work's results, PCL/RA/CeO_2 nanofiber is considered a potential material for drug delivery applications.

Funding

This research received no external funding.

Acknowledgments

The authors are grateful for the provision and supporting facilities by the University Laboratory Management Unit, UTM, Malaysia.

Conflicts of Interest

The authors declare no conflict of interest.

References

1. Fadil, F.; Affandi, N. D. N.; Misnon, M. I.; Bonnia, N. N.; Harun, A. M.; Alam, M. K. Review on electrospun nanofiber-applied products. *Polymers* **2021**, *13*, 2087, https://doi.org/10.3390/polym13132087.
2. Moulefera, I.; Trabelsi, M.; Mamun, A.; Sabantina, L. Electrospun carbon nanofibers from biomass and biomass blends—current trends. *Polymers* **2021**, *13*, 1071, https://doi.org/10.3390/polym13071071.
3. Wang, C.; Wang, J.; Zeng, L.; Qiao, Z.; Liu, X.; Liu, H.; Zhang, J.; Ding, J. Fabrication of electrospun polymer nanofibers with diverse morphologies. *Molecules* **2019**, *24*, 834, https://doi.org/10.3390/molecules24050834.
4. Luraghi, A.; Peri, F.; Moroni, L. Electrospinning for drug delivery applications: A review. *Journal of Controlled release* **2021**, *334*, 463-484, https://doi.org/10.1016/j.jconrel.2021.03.033.

5. Su, Z.; Li, J.; Li, Q.; Ni, T.; Wei, G. Chain conformation, crystallization behavior, electrical and mechanical properties of electrospun polymer-carbon nanotube hybrid nanofibers with different orientations. *Carbon* **2012**, *50*, 5605-5617, https://doi.org/10.1016/j.carbon.2012.08.017.
6. Dong, Z.; Kennedy, S. J.; Wu, Y. Electrospinning materials for energy-related applications and devices. *Journal of Power Sources* **2011**, *196*, 4886-4904, https://doi.org/10.1016/j.jpowsour.2011.01.090.
7. Maghdouri-White, Y.; Bowlin, G. L.; Lemmon, C. A.; Dréau, D. Bioengineered silk scaffolds in 3d tissue modeling with focus on mammary tissues. *Materials Science and Engineering: C* **2016**, *59*, 1168-1180, https://doi.org/10.1016/j.msec.2015.10.007.
8. Liu, H.; Ding, X.; Zhou, G.; Li, P.; Wei, X.; Fan, Y. Electrospinning of nanofibers for tissue engineering applications. *Journal of Nanomaterials* **2013**, *2013*, https://doi.org/10.1155/2013/495708.
9. Yang, C.; Shao, Q.; Han, Y.; Liu, Q.; He, L.; Sun, Q.; Ruan, S. Fibers by electrospinning and their emerging applications in bone tissue engineering. *Applied Sciences* **2021**, *11*, 9082, https://doi.org/10.3390/app11199082.
10. Sedghi, R.; Shaabani, A.; Mohammadi, Z.; Samadi, F. Y.; Isaei, E. Biocompatible electrospinning chitosan nanofibers: A novel delivery system with superior local cancer therapy. *Carbohydrate polymers* **2017**, *159*, 1-10, https://doi.org/10.1016/j.carbpol.2016.12.011.
11. Castillo-Henríquez, L.; Vargas-Zúñiga, R.; Pacheco-Molina, J.; Vega-Baudrit, J. Electrospun nanofibers: A nanotechnological approach for drug delivery and dissolution optimization in poorly water-soluble drugs. *ADMET and DMPK* **2020**, *8*, 325-353, https://doi.org/10.5599/admet.844.
12. Singh, B.; Kim, K.; Park, M.-H. On-demand drug delivery systems using nanofibers. *Nanomaterials* **2021**, *11*, 3411, https://doi.org/10.3390/nano11123411.
13. Zhao, J.; Cui, W. Functional electrospun fibers for local therapy of cancer. *Advanced Fiber Materials* **2020**, *2*, 229-245, https://doi.org/10.1007/s42765-020-00053-9.
14. Arampatzis, A. S.; Kontogiannopoulos, K. N.; Theodoridis, K.; Aggelidou, E.; Rat, A.; Willems, A.; Tsivintzelis, I.; Papageorgiou, V. P.; Kritis, A.; Assimopoulou, A. N. Electrospun wound dressings containing bioactive natural products: Physico-chemical characterization and biological assessment. *Biomaterials research* **2021**, *25*, 1-21, https://doi.org/10.1186/s40824-021-00223-9.
15. Do Pham, D. D.; Jenčová, V.; Kaňuchová, M.; Bayram, J.; Grossová, I.; Šuca, H.; Urban, L.; Havlíčková, K.; Novotný, V.; Mikeš, P. Novel lipophosphonoxin-loaded polycaprolactone electrospun nanofiber dressing reduces staphylococcus aureus induced wound infection in mice. *Scientific reports* **2021**, *11*, 1-15, https://doi.org/10.1038/s41598-021-96980-7.
16. Gouda, M. H.; Ali, S. M.; Othman, S. S.; A Abd Al-Aziz, S.; Abu-Serie, M. M.; Elsokary, N. A.; Elessawy, N. A. Novel scaffold based graphene oxide doped electrospun iota carrageenan/polyvinyl alcohol for wound healing and pathogen reduction: In-vitro and in-vivo study. *Scientific reports* **2021**, *11*, 1-11, https://doi.org/10.1038/s41598-021-00069-0.
17. Malik, S.; Sundarrajan, S.; Hussain, T.; Nazir, A.; Berto, F.; Ramakrishna, S. Electrospun biomimetic polymer nanofibers as vascular grafts. *Material Design & Processing Communications* **2021**, *3*, e203, https://doi.org/10.1002/mdp2.203.
18. Zhang, Y.; Jiao, Y.; Wang, C.; Zhang, C.; Wang, H.; Feng, Z.; Gu, Y.; Wang, Z. Design and characterization of small-diameter tissue-engineered blood vessels constructed by electrospun polyurethane-core and gelatin-shell coaxial fiber. *Bioengineered* **2021**, *12*, 5769-5788, https://doi.org/10.1080/21655979.2021.1969177.
19. Niu, Y.; Galluzzi, M.; Fu, M.; Hu, J.; Xia, H. In vivo performance of electrospun tubular hyaluronic acid/collagen nanofibrous scaffolds for vascular reconstruction in the rabbit model. *Journal of nanobiotechnology* **2021**, *19*, 1-13, https://doi.org/10.1186/s12951-021-01091-0.
20. Sun, Y.; Cheng, S.; Lu, W.; Wang, Y.; Zhang, P.; Yao, Q. Electrospun fibers and their application in drug controlled release, biological dressings, tissue repair, and enzyme immobilization. *RSC advances* **2019**, *9*, 25712-25729, https://doi.org/10.1039/c9ra05012d.
21. Akduman, C.; Özgüney, I.; Kumbasar, E. P. A. Preparation and characterization of naproxen-loaded electrospun thermoplastic polyurethane nanofibers as a drug delivery system. *Materials Science and Engineering: C* **2016**, *64*, 383-390, https://doi.org/10.1016/j.msec.2016.04.005.
22. Aduba Jr, D. C.; Hammer, J. A.; Yuan, Q.; Yeudall, W. A.; Bowlin, G. L.; Yang, H. Semi-interpenetrating network (sipn) gelatin nanofiber scaffolds for oral mucosal drug delivery. *Acta biomaterialia* **2013**, *9*, 6576-6584, https://doi.org/10.1016/j.actbio.2013.02.006.
23. Habibi, Y.; Lucia, L. A.; Rojas, O. J. Cellulose nanocrystals: Chemistry, self-assembly, and applications. *Chemical reviews* **2010**, *110*, 3479-3500, https://doi.org/10.1021/cr900339w.
24. Cerkez, I.; Sezer, A.; Bhullar, S. K. Fabrication and characterization of electrospun poly (e-caprolactone) fibrous membrane with antibacterial functionality. *Royal Society open science* **2017**, *4*, 160911, https://doi.org/10.1098/rsos.160911.
25. Kurakula, M.; Rao, G. K.; Yadav, K. S. Fabrication and characterization of polycaprolactone-based green materials for drug delivery, in *Applications of advanced green materials*. 2021, Elsevier. p. 395-423.
26. Homaeigohar, S.; Boccaccini, A. R. Nature-derived and synthetic additives to poly (ε-caprolactone) nanofibrous systems for biomedicine; an updated overview. *Frontiers in Chemistry* **2022**, *9*, 809676, https://doi.org/10.3389/fchem.2021.809676.

27. Rabionet, M.; Yeste, M.; Puig, T.; Ciurana, J. Electrospinning pcl scaffolds manufacture for three-dimensional breast cancer cell culture. *Polymers* **2017**, *9*, 328, https://doi.org/10.3390/polym9080328.
28. Mondal, D.; Griffith, M.; Venkatraman, S. S. Polycaprolactone-based biomaterials for tissue engineering and drug delivery: Current scenario and challenges. *International Journal of Polymeric Materials and Polymeric Biomaterials* **2016**, *65*, 255-265, https://doi.org/10.1080/00914037.2015.1103241.
29. Repanas, A.; Zernetsch, H.; Glasmacher, B. Core/shell electrospun fibers as biodegradable scaffolds for sustained drug delivery in wound healing applications. *Pneumologie* **2014**, *68*, A85, https://doi.org/10.1055/s-0034-1376854.
30. Li, S.; Dong, S.; Xu, W.; Jiang, Y.; Li, Z. Polymer nanoformulation of sorafenib and all-trans retinoic acid for synergistic inhibition of thyroid cancer. *Frontiers in pharmacology* **2020**, *10*, 1676, https://doi.org/10.3389/fphar.2019.01676.
31. Zhu, Y.-H.; Ye, N.; Tang, X.-F.; Khan, M. I.; Liu, H.-L.; Shi, N.; Hang, L.-F. Synergistic effect of retinoic acid polymeric micelles and prodrug for the pharmacodynamic evaluation of tumor suppression. *Frontiers in pharmacology* **2019**, *10*, 447, https://doi.org/10.3389/fphar.2019.00447.
32. Kim, D. G.; Jeong, Y. I.; Nah, J. W. All-trans retinoic acid release from polyion-complex micelles of methoxy poly (ethylene glycol) grafted chitosan. *Journal of applied polymer science* **2007**, *105*, 3246-3254, https://doi.org/10.1002/app.26480.
33. Szuts, E. Z.; Harosi, F. I. Solubility of retinoids in water. *Archives of Biochemistry and Biophysics* **1991**, *287*, 297-304, https://doi.org/10.1016/0003-9861(91)90482-X.
34. Zhang, X.; Chen, X. Preparation of polyamide 6/ceo2 composite nanofibers through electrospinning for biomedical applications. *International Journal of Polymer Science* **2019**, *2019*, https://doi.org/10.1155/2019/2494586.
35. Kim, J. W.; Mahapatra, C.; Hong, J. Y.; Kim, M. S.; Leong, K. W.; Kim, H. W.; Hyun, J. K. Functional recovery of contused spinal cord in rat with the injection of optimal-dosed cerium oxide nanoparticles. *Advanced Science* **2017**, *4*, 1700034, https://doi.org/10.1002/advs.201700034.
36. Naseri-Nosar, M.; Farzamfar, S.; Sahrapeyma, H.; Ghorbani, S.; Bastami, F.; Vaez, A.; Salehi, M. Cerium oxide nanoparticle-containing poly (ε-caprolactone)/gelatin electrospun film as a potential wound dressing material: In vitro and in vivo evaluation. *Materials Science and Engineering: C* **2017**, *81*, 366-372, https://doi.org/10.1016/j.msec.2017.08.013.
37. Davan, R.; Prasad, R.; Jakka, V. S.; Aparna, R.; Phani, A.; Jacob, B.; Salins, P. C.; Raju, D. Cerium oxide nanoparticles promotes wound healing activity in in-vivo animal model. *Journal of Bionanoscience* **2012**, *6*, 78-83, https://doi.org/10.1166/jbns.2012.1074.
38. Giri, S.; Karakoti, A.; Graham, R. P.; Maguire, J. L.; Reilly, C. M.; Seal, S.; Rattan, R.; Shridhar, V. Nanoceria: A rare-earth nanoparticle as a novel anti-angiogenic therapeutic agent in ovarian cancer. *PloS one* **2013**, *8*, e54578, https://doi.org/10.1371/journal.pone.0054578.
39. Chen, H.; Shi, Y.; Sun, L.; Ni, S. Electrospun composite nanofibers with all-trans retinoic acid and mwcnts-oh against cancer stem cells. *Life Sciences* **2020**, *258*, 118152, https://doi.org/10.1016/j.lfs.2020.118152.
40. Schultze, E.; Ourique, A.; Yurgel, V. C.; Begnini, K. R.; Thurow, H.; de Leon, P. M. M.; Campos, V. F.; Dellagostin, O. A.; Guterres, S. R.; Pohlmann, A. R. Encapsulation in lipid-core nanocapsules overcomes lung cancer cell resistance to tretinoin. *European Journal of Pharmaceutics and Biopharmaceutics* **2014**, *87*, 55-63, https://doi.org/10.1016/j.ejpb.2014.02.003.
41. Ridolfi, D. M.; Marcato, P. D.; Justo, G. Z.; Cordi, L.; Machado, D.; Durán, N. Chitosan-solid lipid nanoparticles as carriers for topical delivery of tretinoin. *Colloids and Surfaces B: Biointerfaces* **2012**, *93*, 36-40, https://doi.org/10.1016/j.colsurfb.2011.11.051.
42. Jia, J. B.; Ling, X.; Xing, M.; Ludwig, J. M.; Bai, M.; Kim, H. S. Novel tspo-targeted doxorubicin prodrug for colorectal carcinoma cells. *Anticancer Research* **2020**, *40*, 5371-5378, https://doi.org/10.21873/anticanres.14545.
43. Recinos, V. R.; Tyler, B. M.; Bekelis, K.; Sunshine, S. B.; Vellimana, A.; Li, K. W.; Brem, H. Combination of intracranial temozolomide with intracranial carmustine improves survival when compared with either treatment alone in a rodent glioma model. *Neurosurgery* **2010**, *66*, 530-537, https://doi.org/10.1227/01.NEU.0000365263.14725.39.
44. Mochane, M. J.; Motsoeneng, T. S.; Sadiku, E. R.; Mokhena, T. C.; Sefadi, J. S. Morphology and properties of electrospun pcl and its composites for medical applications: A mini review. *Applied Sciences* **2019**, *9*, 2205, https://doi.org/10.3390/app9112205.
45. Pillay, V.; Dott, C.; Choonara, Y. E.; Tyagi, C.; Tomar, L.; Kumar, P.; du Toit, L. C.; Ndesendo, V. M. A review of the effect of processing variables on the fabrication of electrospun nanofibers for drug delivery applications. *Journal of Nanomaterials* **2013**, *2013*, https://doi.org/10.1155/2013/789289.
46. Thompson, C.; Chase, G. G.; Yarin, A.; Reneker, D. Effects of parameters on nanofiber diameter determined from electrospinning model. *Polymer* **2007**, *48*, 6913-6922, https://doi.org/10.1016/j.polymer.2007.09.017.
47. Pereira, A. D. F.; Pereira, L. G. R.; Barbosa, L. A. D. O.; Fialho, S. L.; Pereira, B. G.; Patricio, P. S. D. O.; Pinto, F. C. H.; Da Silva, G. R. Efficacy of methotrexate-loaded poly (ε-caprolactone) implants in ehrlich solid tumor-bearing mice. *Drug Delivery* **2013**, *20*, 168-179, https://doi.org/10.3109/10717544.2013.801052.

48. Perumal, G.; Pappuru, S.; Chakraborty, D.; Nandkumar, A. M.; Chand, D. K.; Doble, M. Synthesis and characterization of curcumin loaded pla—hyperbranched polyglycerol electrospun blend for wound dressing applications. *Materials Science and Engineering: C* **2017**, *76*, 1196-1204, https://doi.org/10.1016/j.msec.2017.03.200.
49. Zdraveva, E.; Mijović, B.; Govorčin Bajsić, E.; Slivac, I.; Holjevac Grgurić, T.; Tomljenović, A.; Zubin Ferri, T.; Ujčić, M. Electrospun pcl/cefuroxime scaffolds with custom tailored topography. *Journal of Experimental Nanoscience* **2019**, *14*, 41-55, https://doi.org/10.1080/17458080.2019.1633465.
50. Vasita, R.; Mani, G.; Agrawal, C. M.; Katti, D. S. Surface hydrophilization of electrospun plga micro-/nano-fibers by blending with pluronic® f-108. *Polymer* **2010**, *51*, 3706-3714, https://doi.org/10.1016/j.polymer.2010.05.048.
51. Rychter, M.; Milanowski, B.; Grześkowiak, B. F.; Jarek, M.; Kempiński, M.; Coy, E. L.; Borysiak, S.; Baranowska-Korczyc, A.; Lulek, J. Cilostazol-loaded electrospun three-dimensional systems for potential cardiovascular application: Effect of fibers hydrophilization on drug release, and cytocompatibility. *Journal of colloid and interface science* **2019**, *536*, 310-327, https://doi.org/10.1016/j.jcis.2018.10.026.
52. Hassan, M. I.; Sultana, N. Characterization, drug loading and antibacterial activity of nanohydroxyapatite/polycaprolactone (nha/pcl) electrospun membrane. *3 Biotech* **2017**, *7*, 1-9, https://doi.org/10.1007/s13205-017-0889-0.